



Effect of wire electrode and shielding gas compositions on the mechanical properties of DOMEX 700 steel welded by the GMAW-P process

W. Haupt¹ · K. C. Riffel² · C. L. Israel¹ · R. H. G. Silva² · A. Reguly³

Received: 6 October 2017 / Accepted: 2 March 2018 / Published online: 15 March 2018
© The Brazilian Society of Mechanical Sciences and Engineering 2018

Abstract

High-strength steels such as DOMEX 700 combine high mechanical strength and great ductility. However, when processed by welding their microstructure could present grain growth and deleterious phase formation. Nevertheless, using high-power GMAW-P the effects of electrode and shielding gas composition on the mechanical and microstructure properties of DOMEX 700 welded joints need to be understood. Thus, wire electrodes such as AWS ER 90S-D2 (A1) and AWS ER 120S-G (A2), and shielding gases such as Ar + 15% CO₂ (G1) and Ar + 8% CO₂ (G2) were used and the microstructure of welded joints was analyzed through optical and scanning electron microscope (SEM). Mechanical properties of joints was characterized through joint tensile test, impact test from 20 to – 40 °C, and microhardness in the joint cross-sectional. It is possible to highlight the increase in strength and elongation values with the use of electrode A2, and reduction in impact energy values for specimens welded by gas mixture G2.

Keywords High-power GMAW · High-strength low-alloy steel HSLA · DOMEX 700 · Pulsed MIG/MAG

1 Introduction

There is a high demand for reducing the weight of engineering structures. Therefore, high-strength low-alloy steels (HSLA) are a rather attractive alternative due to their combination of high mechanical strength, good ductility, and high weldability. High-strength low-alloy steels contain microadditions of Nb, Ti, and V, where more refined ferritic–pearlitic microstructure and the hardening capacity by precipitation provide high strength [1]. The carbon content of HSLA steels is reduced to improve weldability

properties [2]. This context introduces the DOMEX 700 steel, which is produced by thermomechanical controlled rolling (TMCR) with heating and cooling cycles, ensuring high mechanical strength allied to excellent material tenacity along with the microaddition of grain refiners and precipitate formers. Due to DOMEX 700 characteristics, this steel is largely applied in the manufacture of cranes for the heavy construction industry.

However, several microstructural changes occur during the welding of these materials, which plays a destructive role in the final mechanical properties of steel. Due to the high-temperature gradient induced in the part during welding, the microstructure is locally modified, reducing its mechanical properties through the increase in grain size, redistribution of precipitates, and formation of fragile microstructure [3].

One of the greatest innovations presented over the last years as an improvement of the GMAW process has been the control of metal transfer, with positive impacts on both process stability and the control of thermal input on the base metal [4]. Such techniques betake both strictly electronic controls, such as waveforms and polarity reversals, and electromechanical control of drop detachments [5, 6]. Thus, over the last years, the industry has striven to

Technical Editor: Márcio Bacci da Silva.

✉ K. C. Riffel
kaueriffel@hotmail.com; kaue.riffel@posgrad.ufsc.br

- ¹ Welding and Metallurgy Laboratory, Department of Mechanical Engineering, University of Passo Fundo, Passo Fundo 90001-970, Brazil
- ² Mechanical Engineering Department, LABSOLDA-Welding and Mechatronics Institute, Federal University of Santa Catarina, Florianópolis 88040-900, Brazil
- ³ Department of Metallurgical Engineering, Federal University of Rio Grande do Sul, Porto Alegre 90040-060, Brazil

improve quality and overcome the limitations of the conventional GMAW process, which led to the development of pulsed arc technologies aiming to improve the application on high-strength steels. The GMAW-P metal transfer is characterized by current pulses between a low level and a high level, so that the mean current of the process is below the spray transfer threshold (transition current) for most applications [7]. Applications with mean current above the transition current are also found today, especially in modern versions of GMAW, benefiting from arc stability and seam formation provided by the pulse mode [8]. The main benefits of the GMAW-P process are significant reduction of thermal input when compared to spray transfer and increase in the deposition rate through the adequate selection of pulse and base parameters [8, 9]. Moreover, it influences cooling rate, metal solidification behavior, and temperature gradients in the heat-affected zone (HAZ), so to improve the mechanical properties of the welded area [9, 10].

However, to ensure such benefits, the GMAW-P process highly depends on the chemical composition of the filler metal, as well as the composition of gas mixture applied as shielding gas [11, 12]. These should have a significant influence in the mechanical and metallurgical properties of the welded joint. The chemical composition of the filler metal directly influences the composition resulting from the weld metal. As for the shielding gas, besides influencing chemical and microstructure composition in a smaller scale, it highly affects the physical characteristics of the electric arc and the weld pool, also resulting in the influence on joint strength properties [13, 14].

This study investigates the effects of two electrodes and two shielding gases on the mechanical properties of joints welded by the GMAW-P process for the DOMEX 700 steel. The main focus and objective of the study is to analyze the variation of mechanical properties for different welding conditions applied, assessing and correlating the results of tensile tests, fusion zone (FZ) impact, and microhardness profile for joints with microstructures present in different areas of the joint.

2 Materials and methods

2.1 Base material and filler metal

The material used in this study was provided by the Swedish Steel Company (SSAB), and produced by controlled rolling with 9.5 mm thickness. Its minimum mechanical properties are 700 MPa (yield strength) and 750 MPa (ultimate tensile strength). Table 1 presents the chemical composition of the base material and Table 2 shows the mechanical properties required for welded joints.

Microadditions of alloy elements that form precipitates are noticed, such as Nb and Ti, as well as the addition of Mn, which increases the mechanical strength by substitutional solid solution [15, 16]. Table 3 presents the compositions of electrodes used, namely electrodes AWS ER 90S-D2 (A1) and AWS ER 120S-G (A2), showing the highest content of Cr and Ni in electrode A2.

The use of these electrodes is justified by DOMEX 700 industrial application. AWS ER 90S-D2 is a welding consumable usually applied in the production lines of cranes, due to its mechanical properties and companies welding procedures. However, the AWS ER 120S-G comes as an alternative, because its higher alloying elements can provide greater quality and properties to the welded joint.

2.2 Welding procedure

The welding process was performed by a 6-axis OTC Daihen Inc. weld robot. The welding source used in the experiment was OTC DP 400. The electrodes used for welding have 1.2 mm of diameter and they should have tensile strength of 620 MPa for A1 and 830 MPa for A2, in the welded condition.

The shielding gases applied in this study were 85% Ar + 15% CO₂ (G1) and 92% Ar + 8% CO₂ (G2), with flow of 14 l/min for all welding conditions. The distance between the contact tip and the part was 15 mm in all conditions, the inclination angle of the welding torch remained at 15° pulling, welding speed was 40 cm/min with triangular structure, amplitude of 2 mm, and frequency of 2 Hz. Table 4 presents the welding conditions assessed in the study, as an experimental matrix.

A synergistic pulsed GMAW program from the OTC source was used for welding, for carbon steel and filler metal, 1.2 mm. In this case, the root pass welding parameters were the following: pulse current (pc) was 300 A, base current (bc) was 48 A, resulting in a mean current (mc) of 170 A; curve pulse times are $t_1 = 0.4$ ms, $t_2 = 1.5$ ms, $t_3 = 0.9$ ms, and $t_4 = 1.5$ ms, resulting in mean voltage of 21.5 V for gas (G1) and 20.3 V for gas (G2) at wire speed of 5.1 m/min. The same synergistic curve was used for the filler pass, but with higher mean current set by the operator. Therefore, the pulsed wave parameters were the following: pc of 450 A, bc of 60 A, and resulting in a mc of 250 A; pulse times were $t_1 = 0.6$ ms, $t_2 = 1.8$ ms, $t_3 = 1.2$ ms, and $t_4 = 1.8$ ms, resulting in mean voltage of 26.2 V for mixture (G1) and 25.4 V for mixture (G2) at wire speed of 7.4 m/min. The parameters were acquired with the system available in the welding robot cell, which shows voltage and welding current in real time.

The dimensions of specimens used in the experiment were 200 × 100 × 9.5 mm and welding direction was

Table 1 Chemical composition of the base material

C	Si	Mn	P	Cr	Mo	Ni	Ti	V	Nb	W
0.0283	0.0568	1.84	0.0132	0.0391	0.0821	0.0327	0.148	0.0093	0.0586	0.015

Table 2 Standardized mechanical properties for DOMEX 700 welded joints

Yield strength (MPa)	Ultimate tensile strength (MPa)	Elongation min %
700	750–950	12

Table 3 Chemical composition of filler metals used

Electrode	C	Si	Mn	P	S	Cr	Mo	Ni	V	Ti
A1	0.07–0.12	0.50–0.80	1.60–2.10	0.025	0.025	–	0.40–0.60	0.15	–	–
A2	0.1	0.25–0.60	1.40–1.80	0.010	0.010	0.60	0.3–0.65	2.0–2.80	0.03	0.10

Table 4 Experimental matrix of welding parameters

Weld condition	Electrode	Shielding gas
A	A2	G1
B	A2	G2
C	A1	G1
D	A1	G2

perpendicular to base material rolling. A V-shaped joint with 60° bevel angle, 2 mm root opening, and 1.5 mm nose height was used in all welding conditions.

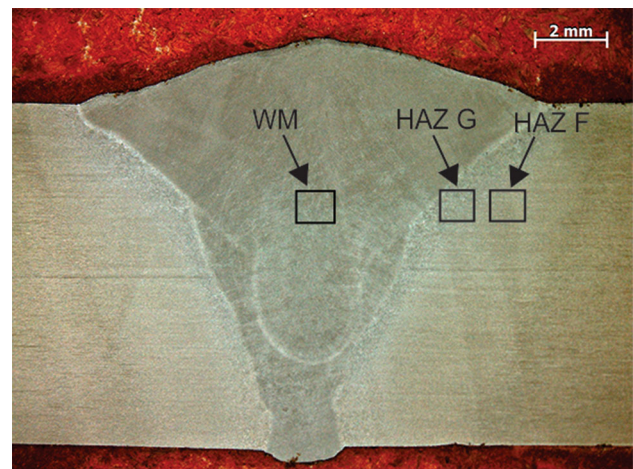
2.3 Metallurgical analysis

2.3.1 Macrostructure analysis

The cross-sectional macrostructure analysis of the weld seam was performed by embedding specimens in Bakelite resin, sequential grinding from the 220 to the 1200-grit paper, and polishing with 1 μm alumina. Etching was performed by immersion in 10% Nital etchant solution for 20 s. Images were obtained in ZEISS model Stemi 2000-C stereo microscope.

2.3.2 Microstructure analysis

A scanning electron microscope (SEM) of the Tescan VEGA3 LM brand was used for microstructure analysis. For preparation, the samples were cut with a cooled saw blade, embedded in Bakelite resin, and then subjected to sequential grinding with grit paper ranging from 220 to 2500, polished with 1 μm alumina, and etched with 10% Nital solution for 20 s. The microstructures assessed were in the weld metal (WM), coarse grain heat-affected zone (HAZ G) and fine grain heat-affected zone (HAZ F). The specific areas are shown in Fig. 1.

**Fig. 1** Microstructure analysis areas

2.4 Mechanical tests

2.4.1 Tensile test

To determine the tensile strength of base metal and welded joints, specimens were obtained according to the ASTM E8M standard [17], perpendicular to the welded joint. Three specimens were tested for each welding condition and base material, and the weld seam reinforcement was maintained for the welded condition. The test was performed in a universal testing machine of the brand INSTRON model 5585H, under a loading rate of 0.75 mm/min. Deformation was measured during the test by an extensometer of the brand INSTRON model Cat. N. 2630-106, the length of the reduced specimen section was 50 mm, and the gauge length of the extensometer was 25 mm.

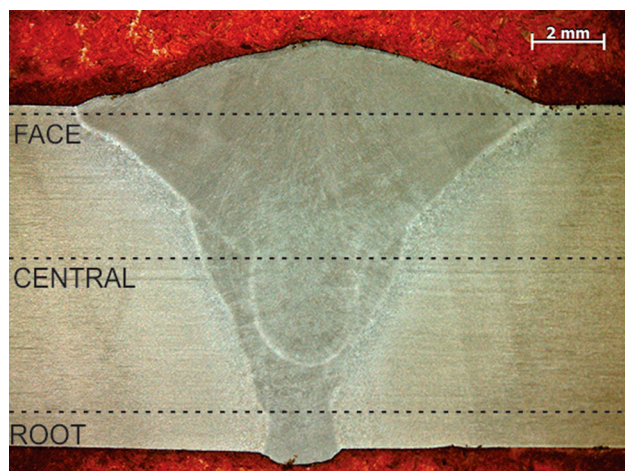


Fig. 2 Microhardness profile lines

2.4.2 Impact test

For determining the impact energy absorbed by the welded joints, Charpy-V impact tests were performed according to the ASTM E 23-16 standard [18], at temperatures of 20, 0, -20 , and -40 °C for each welded condition, and a ductile–fragile transition curve was produced for different welding conditions. The notch was positioned along the side of the specimen in the fusion zone (FZ) area of the welded materials. The equipment used in the Charpy-V test was of the HECKERT brand, and samples were cooled in liquid nitrogen and remained immersed for 15 min to

homogenize temperatures in the section. A thermocouple of the brand Elcometer model 213 was used for measuring the temperature during the test, at temperatures ranging from -50 to 850 °C and 1 °C resolution.

2.4.3 Microhardness profile of joints

Microhardness was mapped in different areas of the welded joints with a microhardness tester SHIMADZU model HMV-G 20ST. The test was set at 0.3 kgf loading with 0.3 mm distance between indentations, according to the ASTM E 384-16 standard [19]. Microhardness profiles were performed along the areas of the sectioned face of the weld seam, including a profile along the face of the seam, central area, and joint roots. Figure 2 presents the microhardness profile position in the cross-section.

3 Results

3.1 Macrographic analysis

The characterization of the cross-section of the deposited seam presented welds with complete penetration in all conditions, as shown in Fig. 3. A good appearance of the weld seam for all conditions was observed, in terms of weld bead reinforcement and wettability.

Fig. 3 Macrograph of joints produced. **a** Electrode AWS ER 120S-G gas G2 85% Ar + 15% CO₂, **b** electrode AWS ER 120S-G gas G1 92% Ar + 8% CO₂, **c** electrode AWS ER 90S-D2 gas G2 85% Ar + 15% CO₂, and **d** electrode AWS ER 90S-D2 gas G1 92% Ar + 8% CO₂

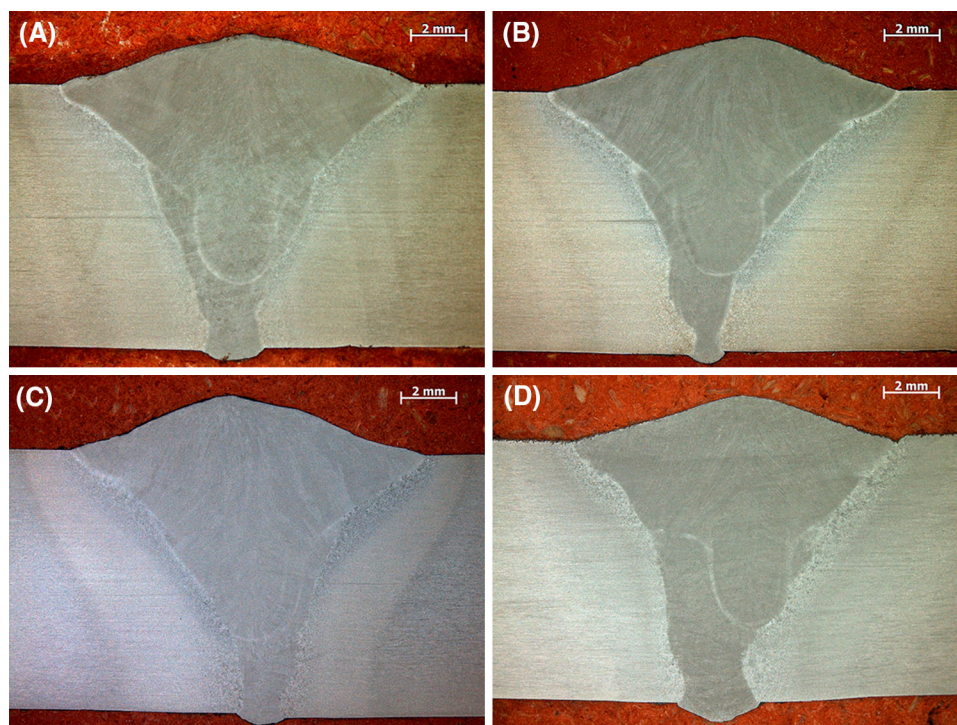
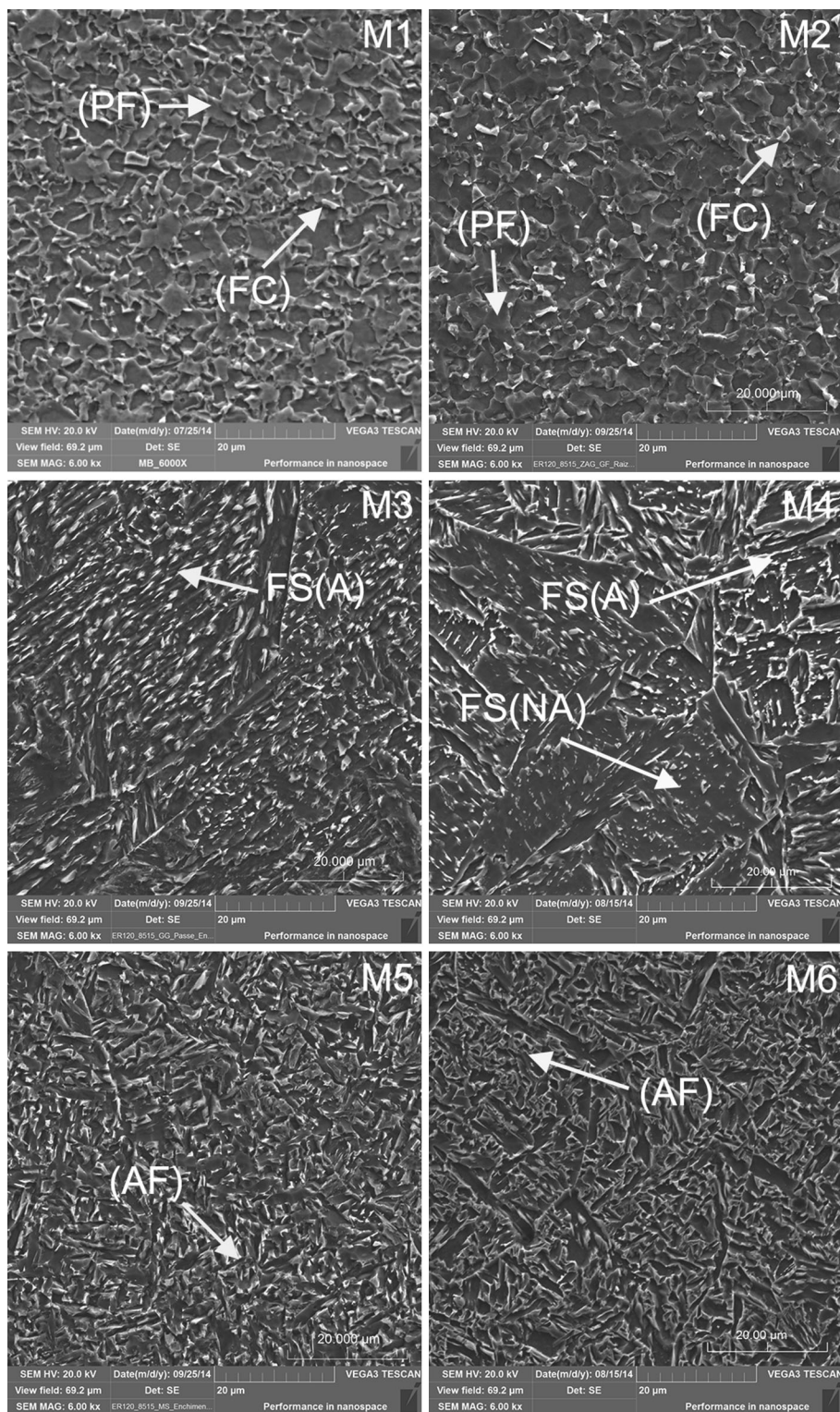


Fig. 4 Microstructure of base material and welded joints (M1–M6)



3.2 Microstructure analysis in SEM

The microstructural analysis in Fig. 4 indicated a significant increase in grain size along the heat-affected zone, from the heat produced during welding. It is possible to

verify the formation of Widmanstätten ferrite with aligned microphase-FS (A) and Widmanstätten ferrite with non-aligned microphase-FS (NA) in this area. Thus, there was an increase in grain size around weld metal, providing the Widmanstätten ferrite formation which is very common in

Fig. 5 Results of the tensile test of base material and the different welding conditions

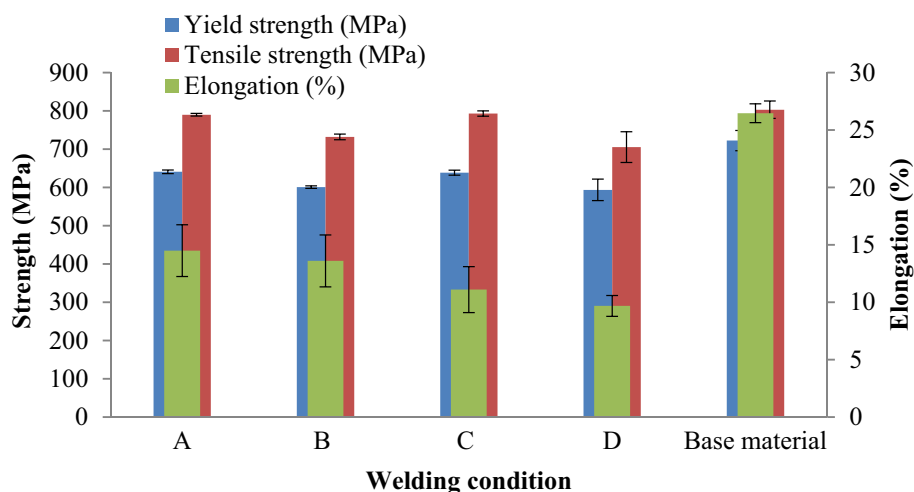


Table 5 Mean values of yield strength and tensile strength

Weld condition	Yield strength (MPa)	Tensile strength (MPa)	Elongation (%)
A	650	790	15
B	610	760	12
C	640	800	11
D	610	730	9
Base material	730	810	27

this zone. Thewlis [20] has shown the Widmanstätten ferrite formation in the HAZ of HSLA welded joints, where it was used in GMAW process. In the case, this phase contributed to reduction of mechanical properties.

The filler metal area is mostly composed by acicular ferrite (AF), which is a phase encountered in microalloyed steel-melted zone. Researches have presented similar results in welding of HSLA, with acicular ferrite formation in melted zone [21, 22].

Figure 4 (M1 and M2) shows the base material and the heat-affected zone with grain refining, respectively, which present polygonal ferrite (PF) as main constituent and areas with ferrite-carbide aggregates (FC). Figure 4 (M3 and M4) presents the HAZ areas of welds A and B, where grain development and presence of Widmanstätten ferrite with aligned and non-aligned microphases [FS (A) and FS (NA)] may be observed. Figure 4 (M5 and M6) presents images of the fusion zone of welds A and B with the presence of acicular ferrite (AF).

3.3 Mechanical tests

3.3.1 Joint tensile test

Figure 5 and Table 5 present the values of properties of yield strength (MPa), tensile strength (MPa), and elongation (%) for different welding conditions and base material; it is worth noting there was rupture along the HAZ area for

all welded conditions, highlighting the reduction in elongation values relative to the base material, indicating a ductility loss caused by grain development and local microstructure changes.

Welding condition A presented the best results regarding tensile strength and elongation, with a reduction of 1.6% in maximum strength and of 45.2% in elongation, when compared to base material. Welding condition B presented a reduction of 8.8% in σ_{uts} and 48.6% in elongation. Condition C showed a reduction of 1.2% in σ_{uts} and 58.0% in elongation. Condition D showed a reduction of 12.1% on σ_{uts} and 63.4% in elongation when compared to the base material. It is possible to verify a reduction in elongation values when using gas mixture G2, resulting in 23.3% when applying electrode A2 and 28.8% when using electrode A1.

However, tensile strength values decreased when applying electrode A1, due to the lower content of alloy elements present in this electrode. The A2 electrode presents higher content of alloy elements than electrode A1, as Cr and Ni, increasing the mechanical strength and tenacity. Also, the higher presence of Ti and V in A2 forms carbides which justifies the mechanical strength increase.

3.3.2 Weld impact test

The impact tests showed a clear tendency to reduce the energy absorbed by applying shielding gas G2 (B and D) at

lower temperatures, presenting lower energy values at low temperatures relative to shielding gas G1 (A and C); the graphs of Fig. 6 present such reduction.

This tendency evidences a reduction of tenacity by applying the gas with lower oxidizing content. Such fact may be attributed to better electric arc stability using gas mixture G1, which allowed the material to improve deposition conditions. This may have occurred because of the phenomenon of stabilization of cathode points over the pool, increasing arc rigidity [23, 24]. It is known that such a result confronts previous studies in the literature in which authors affirm that tenacity reduces as the level of CO₂ increases [11, 14]. However, such studies do not exclusively mention pulsed current welding, which is the waveform used in this work. Moreover, the base material hereby used is also a differential, because of the high content of alloy elements and the low rate of carbon in it (about 0.03%). Thus, this hypothesis is more appropriate for the results hereby obtained to differ from publications in the field.

The different electrodes do not influence the impact results in the weld metal area. It is also possible to report a

small variation in arc tensile values when applying different welding gases. Higher tensile values were verified for mixture G1, which increased welding energy and may have reduced the cooling speed of joints, affecting energy impact values. Also, the higher amount of Ni available in electrode A2, increases the weld metal tenacity. This behavior in HSLA welded joints is also presented by Pamnani [25] in his study.

The fractographs presented in Fig. 7 show the change of fracture mode from dimples, which is a ductile fracture (A and C), to cleavage, indicating a brittle fracture (B and D), with the change in the shielding gas.

Figure 7 presents, respectively, the fracture surface of specimens with lower impact energy for welds. The test temperature for the surfaces of the figure was $-20\text{ }^{\circ}\text{C}$, recording the respective energies absorbed as 132, 47, 102 and 34 J.

3.3.3 Weld microhardness profile

The microhardness profile presents a hardness reduction along the HAZ area, which showed recrystallization and

Fig. 6 Impact strength in different welding conditions

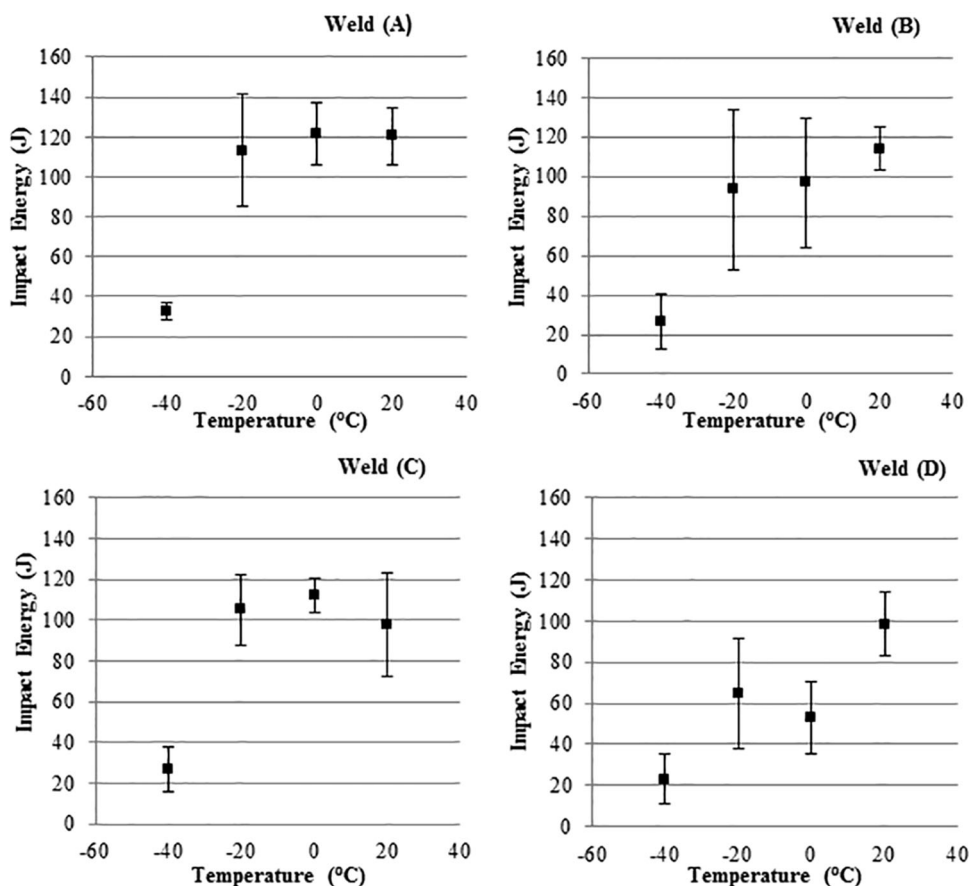
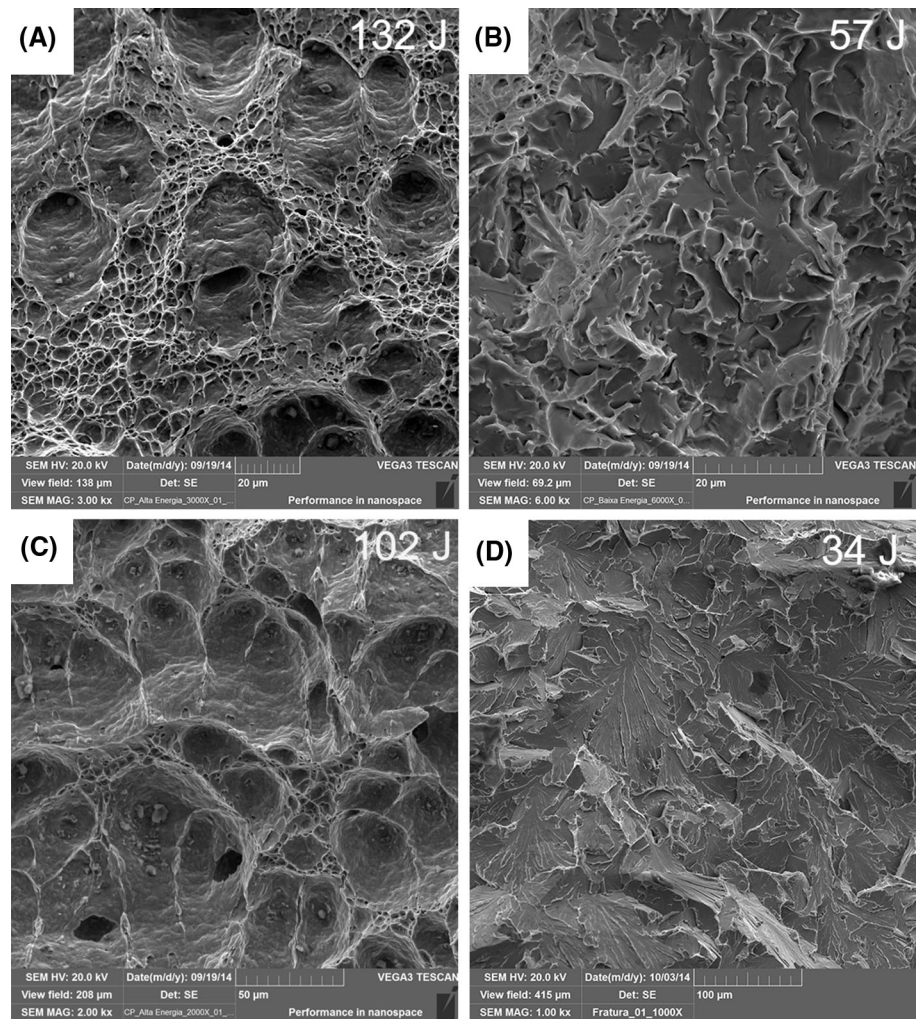


Fig. 7 Impact test of the fracture surface at $-20\text{ }^{\circ}\text{C}$ for welding conditions. **a** Weld A: $\times 3000$; **b** weld B: $\times 6000$; **c** weld C: $\times 2000$; **d** weld D: $\times 1000$



grain development of the material with internal tensile relief in the area, thus reducing hardness and mechanical strength, as presented in Fig. 8.

It is possible to show that electrode AWS ER 120 S-G (Weld A and B) in Fig. 8 maintained higher hardness in the HAZ area and in the weld metal, when compared to AWS ER 90 S-D2 (Weld C and D) both showed in Fig. 9. This is due to the presence of alloy elements such as Cr and Ni in the filler metal, which maintained higher hardness values recorded in this area.

When applying electrode AWS ER 90 S-D2, a greater hardness reduction is verified in the weld metal and HAZ, due to the lower content of alloy elements present in this electrode, according to Fig. 9 in weld C and D.

It is also possible to verify a significant influence of shielding gases on microhardness profile. Whereas, the application of gas mixture G2 (Weld D) shows higher homogeneity of microhardness values along the cross-

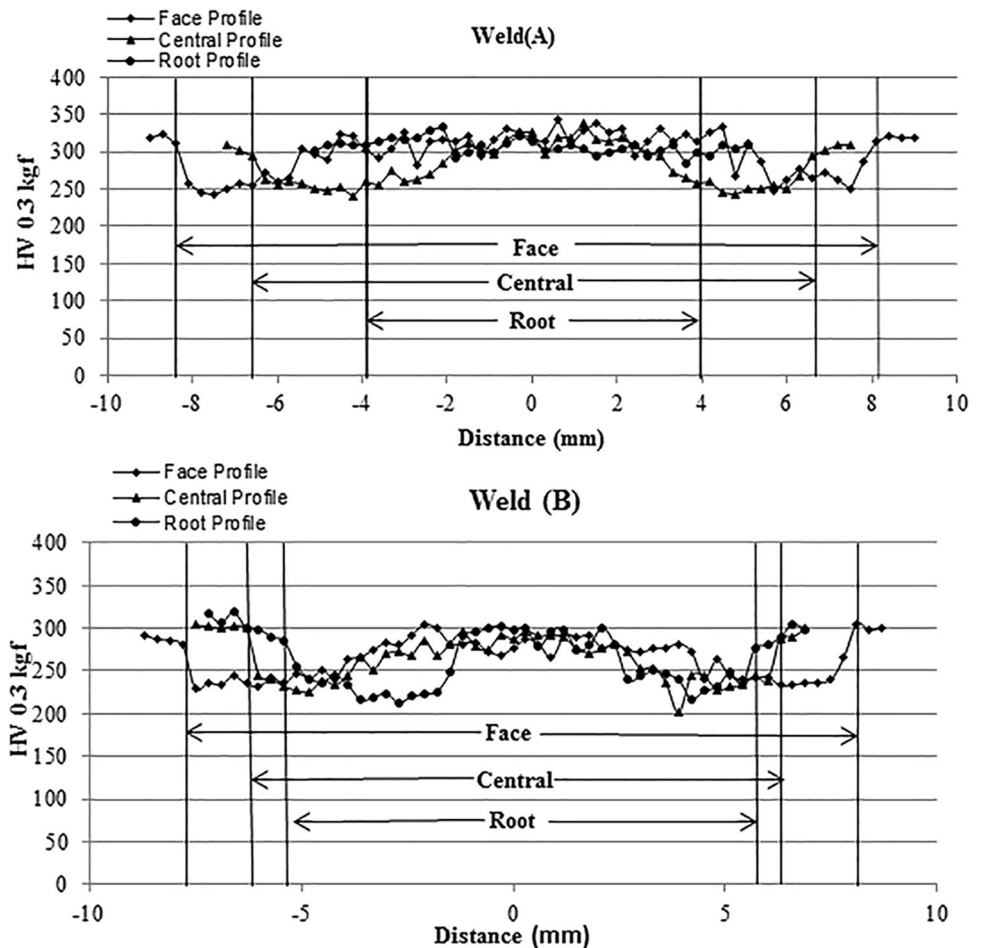
section. The higher oxidizing content of the shielding gas may have increased hardness in the weld metal and the HAZ and increased tenacity along the HAZ (Weld C), as recorded in the impact test.

4 Conclusion

When studying the effects of composition of electrodes and shielding gas applied in welding of DOMEX 700 steel, it is possible to verify that:

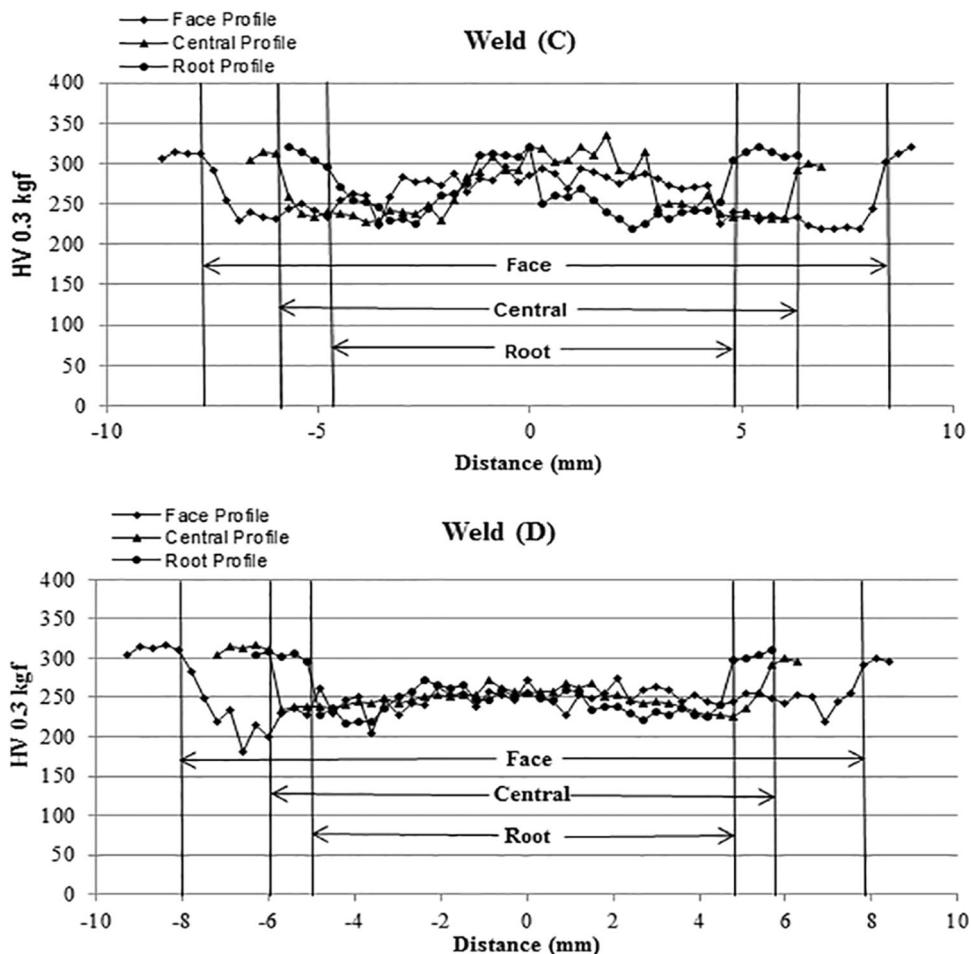
- Applying electrode AWS ER 120S-G allowed higher mechanical strength and elongation values for welded joints in comparison with electrode AWS ER 90S-D2, using the same gas for both. This is due to the higher contents of alloy elements present in this electrode AWS ER 120S-G, such as Cr and Ni;

Fig. 8 Welded joints microhardness profile using AWS ER 120 S-G



- There was greater electric arc stability with the use of gas mixture G1, with higher CO₂ content, when compared to gas mixture G2;
- The weld metal area presented acicular ferrite (AF) microstructure, while the HAZ area presented grain development and formation of Widmanstätten ferrite with aligned and non-aligned microphases [FS (A) and FS (NA)];
- The impact strength values at low temperatures were higher for joint welded by gas mixture G1, where CO₂ values are higher than the gas mixture G2;
- The hardness values in the different joint areas are influenced by electrodes where electrode AWS ER 120S-G obtained the highest hardness values;
- The shielding gas has affected the hardness values, whereas the use of gas mixture G1 presented higher

Fig. 9 Welded joints microhardness profile using AWS ER 90 S-D2



hardness values, and the use of gas G2 with lower CO₂ contents presented greater homogeneity in hardness values.

Acknowledgements The authors would like to acknowledge the financial support of CAPES and CNPq.

References

1. Koo JY, Luton MJ, Bangaru NV, Petkovic RA (2003) Metallurgical design of ultra-high strength steels for gas pipelines. In: International offshore and polar engineering conference. ISBN 1-880653-60-5 (Set); ISSN 1098-6189 (Set), Honolulu, Hawaii, USA, May 25–30, 2003
2. Pickering FB (1975) High-strength, low-alloy steels—a decade of progress. In: Micro-alloying 75, proceedings. Union Carbide Corp., New York, p 9
3. Ramazani A, Mukherjee K, Abdurakhmanov A, Prahl U, Schleser M, Reisgen U, Bleck W (2014) Micro-macro-characterisation and modelling of mechanical properties of gas metal arc welded (GMAW) DP600 steel. *Mater Sci Eng A* 589:1–14
4. Cuiuri D, Norrish J, Cook CD (2002) New approaches to controlling unstable gas metal arc welding. *Australas Weld* 47(3):39–47
5. Dutra JC, Silva RHG, Savi BM, Marques C, Alarcon OE (2015) Metallurgical characterization of the 5083H116 aluminum alloy welded with the cold metal transfer process and two different wire-electrodes (5183 and 5087). *Weld World* 59:797–807
6. Dutra JC, Silva RHG, Marques C (2016) A new approach for MIG/MAG cladding with Inconel 625. *Weld World* 60:1201–1209
7. Praveen P, Yarlagadda PKDV, Kang MJ (2005) Advancements in pulse gas metal arc welding. *J Mater Process Technol* 164–165:1113–1119
8. Stol I, Williams KL, Gaydos D (2006) Back to basics: using a buried gas metal arc for seam welds. *Weld J* 85(4):28
9. Mirzaei M, Jeshvaghani RA, Yazdipour A, Madar KZ (2013) Study of welding velocity and pulse frequency on microstructure and mechanical properties of pulsed gas metal arc welded high strength low alloy steel. *Mater Des* 51:709–713
10. Devakumaran K, Ghosh PK (2010) Thermal characteristics of weld and HAZ during pulse current gas metal arc weld bead deposition on HSLA steel plate. *Mater Manuf Process* 25:616–630
11. Kulkarni SG, Ghosh PK, Ray S (2008) Improvement of weld characteristics by variation in welding processes and parameters in joining of thick wall 304 LN stainless steel pipe. *ISIJ Int* 48:1560–1569
12. Wu CS, Chen MA, Lu YF (2005) Effect of current waveforms on metal transfer in pulsed gas metal arc welding. *Meas Sci Technol* 16(12):2459

13. Lu L, Fan D, Huang J, Shi Y (2012) Decoupling control scheme for pulsed GMAW process of aluminum. *J Mater Process Technol* 212:801–807
14. Stenbakca N, Persson K (1989) Shielding gases for gas metal arc welding. *Weld J Miami* 8(11):41–47
15. Gladman T (1997) The physical metallurgy of microalloyed steels. The Institute of Metals, London, pp 349–357
16. Pereloma E, Edmonds DV (eds) (2012) Phase transformation in steel. Volume 1: fundamentals and diffusion-controlled transformations. Woodhead Publishing Limited, Oxford, pp 157–183
17. ASTM E8/E8M-16a (2016) Standard test methods for tension testing of metallic materials. ASTM International, West Conshohocken
18. ASTM E23-16b (2016) Standard test methods for notched bar impact testing of metallic materials. ASTM International, West Conshohocken
19. ASTM E384-16b (2016) Standard test methods for notched bar impact testing of metallic materials. ASTM International, West Conshohocken
20. Thewlis G (2004) Classification and quantification of microstructures in steels. *Mater Sci Technol* 20:143–160
21. Zhang C, Yang J, Hu X, Lu P, Zhao M (2012) Microstructure characteristics and fatigue properties of welded HSLA with and without buffer layer. *Mater Sci Eng A* 546:169–179
22. Jing-hong Y, Qing-you L, Dong-bai S, Xiang-yang L (2010) Microstructure and transformation characteristics of acicular ferrite in high niobium-bearing microalloyed steel. *J Iron Steel Res Int* 17(6):53–59
23. Vaidya V (2002) Shielding gas mixtures for semiautomatic welds. *Weld J Miami* 81(9):43–48
24. Costa MCMS, Starling CMD, Modenesi PJ (2010) Characterization of GMAW arc instability phenomena related to low oxidation potential shielding gases. *Weld Int* 24(3):214–221
25. Pamnani R, Jayakumar T, Vasudevan M, Sakthivel T (2016) Investigations on the impact toughness of HSLA steel arc welded joints. *J Manuf Process* 21:75–86